THE JOURNAL OF BIOLOGICAL CHEMISTRY VOL. 288, NO. 26, pp. 19050–19059, June 28, 2013

Dynamin Isoforms Decode Action Potential Firing for Synaptic Vesicle Recycling*

Received for publication, December 17, 2012, and in revised form, May 14, 2013 Published, JBC Papers in Press, May 16, 2013, DOI 10.1074/jbc.M112.445874

Shota Tanifuji[‡§], **Megumi Funakoshi-Tago**[§], **Fumihito Ueda**[§], **Tadashi Kasahara**[§], **and Sumiko Mochida**[‡1]

From the [‡]*Department of Physiology, Tokyo Medical University, Tokyo 160-8402, Japan and the* [§]*Department of Biochemistry, Keio University, Minato-ku, Tokyo 105-8512, Japan*

Background: The molecular mechanism linking variation in presynaptic neuronal activity to vesicle trafficking is unknown.
Results: Three isoforms of dynamin, an essential endocytic protein, mediate vesicle reuse, having distinct rate and time constants with physiological action potential frequencies.
Conclusion: Dynamin isoforms select appropriate vesicle reuse pathways associated with specific neuronal firing patterns.
Significance: Individual dynamin isoforms regulate distinct synaptic vesicle reuse pathways that cover the full range of physiological action potential frequencies.

Presynaptic nerve terminals must maintain stable neurotransmission via synaptic vesicle membrane recycling despite encountering wide fluctuations in the number and frequency of incoming action potentials (APs). However, the molecular mechanism linking variation in neuronal activity to vesicle trafficking is unknown. Here, we combined genetic knockdown and direct physiological measurements of synaptic transmission from paired neurons to show that three isoforms of dynamin, an essential endocytic protein, work individually to match vesicle reuse pathways, having distinct rate and time constants with physiological AP frequencies. Dynamin 3 resupplied the readily releasable pool with slow kinetics independently of the AP frequency but acted quickly, within 20 ms of the incoming AP. Under high-frequency firing, dynamin 1 regulated recycling to the readily releasable pool with fast kinetics in a slower time window of greater than 50 ms. Dynamin 2 displayed a hybrid response between the other isoforms. Collectively, our findings show how dynamin isoforms select appropriate vesicle reuse pathways associated with specific neuronal firing patterns.

Neurons in both central and peripheral nervous systems encounter a wide range of activity in the form of action potential (AP)[2] firing patterns. In accord, membrane transport systems, in particular synaptic vesicle (SV) recycling pathways in synapses that mediate fast neurotransmission, must maintain the ability to react rapidly to ongoing changes in AP firing and adjust membrane trafficking to provide sufficient membrane replenishment. SV recycling through repetitive cycles of exocytosis and endocytosis is well established to operate under different conditions of synaptic activity and is typically classified for fast synapses by imaging and electrophysiology into fast and slow modes (1), whereas morphologically retrieval is usually described as "kiss-and-run" fusion/fission, full-collapse vesicle retrieval, and bulk modes (2–4). The relationship between the kinetic phases with morphological retrieval is a matter of ongoing debate and may depend on the particular synapse.

The slow mode of endocytosis is mediated by the classic clathrin-mediated pathway (3) and is responsible for refilling of the readily releasable pool (RRP) via a reserve pool (RP) (5). In contrast, the fast mode of endocytosis involves the rapid reuse of SVs that bypasses the RP (2, 6, 7). In addition to these modes of SV recycling, bulk endocytosis is also rapidly triggered during strong stimulation (8–10), although its contribution to the RRP is unknown. The molecular mechanism for the selection of a specific pathway for membrane trafficking during dynamic changes in AP properties is poorly understood.

A candidate mechanism for SV recycling indexed to cell activity could involve a protein central to endocytosis. Most forms of endocytosis in the physiological range require the protein dynamin, a GTPase that mediates fission of SVs from the presynaptic terminal membrane (11). There are three dynamin isoforms (12, 13). Dynamin 1 and 3 are highly expressed in brain, whereas dynamin 2 is ubiquitous (12, 14). Knockout of dynamin 1 and 3 in central neurons suggests that dynamin 1 is required for fast SV recycling with high-frequency stimulation (13, 15) and that dynamin 2 may control SV recycling after stimulation (13). In these studies, dynamin 3 has no direct effect on SV endocytosis but cooperates with dynamin 1 to support optimal rates of SV endocytosis (15). Other studies show that measurements of SV recovery after stimulation indicate that dynamin promotes RRP maintenance. Synaptic fatigue following high-frequency AP firing is observed at the calyx of Held in the presence of a dynamin inhibitor (16) and in *Drosophila* mutant flies carrying a temperature-sensitive allele of dynamin (*Drosophila shibire*) at the non-permissive temperature (17). However, although these studies collectively establish a general role for dynamin and its isoforms in membrane recycling, several important questions remain unanswered.

Here, we examined the role of dynamin isoforms in activity sensing in a model system for the genetic analysis of fast cholinergic transmission between rat superior cervical ganglion

* This work was supported by grants-in-aid for scientific research B and for exploratory research (to S. M.).
[1] To whom correspondence should be addressed: Department of Physiology, Tokyo Medical University, Tokyo 160-8402, Japan. E-mail: mochida@tokyo-med.ac.jp.
[2] The abbreviations used are: AP, action potential; SVs, synaptic vesicles; RRP, readily releasable pool; RP, reserve pool; SCG, superior cervical ganglion; RRSV, release ready synaptic vesicle; EPSP, excitatory postsynaptic potential; ISI, interstimulus interval; ANOVA, analysis of variance; KD, knockdown.

(SCG) neurons (18–20). Dynamin isoforms were specifically knocked down in presynaptic neurons by microinjection of siRNA. The transfected neurons were challenged with various AP firing patterns, and the resultant changes in the recovery of release-ready SVs (RRSVs) in the RRP were monitored by recording evoked excitatory postsynaptic potentials (EPSPs). We discovered that individual dynamin isoforms are associated with distinct patterns of RRP recruitment, suggesting their ability to sense cell activity and regulate distinct SV recycling pathways that cover the full range of physiological AP frequency.

EXPERIMENTAL PROCEDURES

Ethical Approval

The Ethics Committee of Tokyo Medical University approved this project.

Plasmids

N-terminal HA-tagged murine dynamin 1, N-terminal FLAG-tagged murine dynamin 2, and N-terminal Myc-tagged dynamin 3 were subcloned into MSCV-IRES-PURO.

siRNA

Dynamin 1, 2, 3 or control negative siRNA (catalog nos. sc-35234, sc-35237, sc-41209, and sc-36869, Santa Cruz Biotechnology, Santa Cruz, CA) were used.

Antibodies

Anti-HA antibody (Roche Diagnostics Japan, Tokyo, Japan), anti-FLAG antibody (catalog no. m2, Sigma-Aldrich Japan, Tokyo, Japan), anti-Myc-antibody (catalog no. 9E10, Santa Cruz Biotechnology), and anti-dynamin 1, 2, 3 or 1–3 antibody (catalog nos. sc-12724, sc-6400, sc-69472, or sc-11362, Santa Cruz Biotechnology) were used.

HEK293T Cell Culture and Transfection

HEK293T cells were cultured in DMEM containing 10% fetal bovine serum, 2 mM glutamine, and 100 units each of penicillin and streptomycin (Life Technologies Corp., Japan, Tokyo). HEK293T cells were transfected with 1 μg of MSCV-Puro-N-HA-dynamin-1, MSCV-Puro-N-FLAG-dynamin-2, and MSCV-Puro-N-Myc-dynamin-3 with 100 pM of control siRNA or siRNAs against dynamin 1, 2, or 3 using FuGENE 6 (Roche Diagnostics Japan).

PC12 Cell Culture and Transfection

PC12 cells were cultured in DMEM containing 10% fetal bovine serum, 5% horse serum, and 100 units each of penicillin and streptomycin (Life Technologies Corp.). The day before transfection, PC12 cells were plated in culture medium without antibiotics and transfected with siRNA against dynamin 1, 2, 3, or control negative siRNA (100 pM) using Lipofectamine 2000 (Life Technologies Corp.).

Immunoblotting

After 48 h of transfection, HEK293T cells and PC12 cells were harvested in ice-cold PBS and lysed in Nonidet P-40 lysis buffer (50 mM Tris-HCl (pH 7.4), 10% glycerol, 50 mM NaCl, 0.5% sodium deoxycholate, 1% Nonidet P-40, 20 mM NaF, 0.2 mM Na_3VO_4) supplemented with protease inhibitors. Cell lysates from postnatal day 7 Wistar ST rat brain prepared using Nonidet P-40 lysis buffer or from HEK293T cells and PC12 cells were resolved by SDS-PAGE and transferred to PVDF membranes. Membranes were probed by using the designated antibodies and visualized with the ECL detection system (GE Healthcare Japan, Tokyo).

Neuronal Culture and Transfection

Postnatal day 7 Wistar ST rats of either sex were decapitated under diethylether anesthesia according to the guidelines of the Physiological Society of Japan. Isolated SCG neurons were cultured for 5–7 weeks (21) and microinjected (22) with dynamin 1, 2, 3, or control negative siRNA. To monitor the injected amount and to detect injected neurons, siRNA was introduced with dextran fluorescein 10,000 MW (catalog no. D-1820, Molecular Probes, Eugene, OR). The reduction in dynamin expression was confirmed by a decrease in fluorescence intensity of immunocytochemical staining (Fig. 1, *E–H*) (22).

Immunostaining

Three days after siRNA injection, SCG neurons were stained as described (22). Anti-dynamin 1, 2, or 3 antibody (1:50) was used for the primary antibody. Alexa Fluor 546 rabbit anti-mouse IgG or Alexa Fluor 546 donkey anti-goat IgG (A-catalog nos. 11060 or A-11056, 1:500, Molecular Probes) was used for the secondary antibody. Confocal images were obtained with a Nikon EZ-C1 microscope using a water immersion ×60 objective. Images of dynamin 1, 2, and 3 in the siRNA-injected and adjacent non-injected neurons were acquired using the same settings below saturation at a resolution of 1024 × 1024 pixels (12-bit), and the density of dynamin 1, 2, and 3 was quantified by averaging fluorescence intensity within three circles (50 μm^2 each) in the cytoplasm of a siRNA-injected neuron and an adjacent non-injected neuron using the MetaMorph software (Molecular Devices, Sunnyvale, CA). The regions of interest for comparison of fluorescence intensity between siRNA-injected and non-injected neurons in an image were chosen randomly, and overlap with the nucleus in the cell body was avoided.

Electrophysiology

Presynaptic neurons three to four days after siRNA injection (22) or immediately after anti-dynamin 1, 2, 3, 1–3, or control antibody injection (23) were used. Neurons were superfused with a modified Krebs solution consisting of 136 mM NaCl, 5.9 mM KCl, 2.5 mM $CaCl_2$, 1.2 mM $MgCl_2$, 11 mM glucose, and 3 mM Na-HEPES (pH 7.4, 32–34 °C) (24). Presynaptic APs were generated by passing current through a sharp recording electrode filled with 1 M K-acetate (70–90 MΩ), and EPSPs were recorded from a neighboring non-transfected neuron. Data were collected using Clampex 10.2 (Molecular Devices, Downtown, PA).

Data Analysis

Collected data were analyzed with Origin software (OriginLab, Northampton, MA).

Paired-pulse Ratio—Two consecutive APs at various interstimulus intervals (ISIs) were elicited in a siRNA-injected neuron every 1 min (n = 5–13). Three recordings for each ISI were

performed. To calculate the paired-pulse ratio, the second EPSP amplitude measured from the end of the first EPSP was divided by the amplitude of the first EPSP measured from the base line before generating the first EPSP. The mean values of the paired-pulse ratio for individual synapse were averaged.

EPSPs with High-frequency AP Trains—To measure the reduction of RRSVs in response to high-frequency AP firing, 2-s AP trains at 5, 10, and 20 Hz were elicited consecutively (n = 4–6), and three recordings of EPSPs for each frequency AP train were performed every 2 min. To compare the recovery of RRSVs from the 2-s AP train stimulation, the peak amplitude of the first EPSP in response to each frequency train was normalized to the peak amplitude of the first EPSP at the 5 Hz AP train. To compare the amount of neurotransmitter released from RRSVs during 2-s AP trains, EPSP integral values were calculated from regions over the base line of EPSP traces using Origin 8 "Area." To compare the responsiveness of RRSVs to 2-s AP trains, the number of EPSP failures was counted during the first 10 APs of individual 2-s trains. To compare the reduction of RRSVs during 2-s trains, the peak amplitude measured from the end of the previous EPSP was normalized to the first EPSP amplitude measured from the base line of EPSP traces. To compare the number of RRSVs before applying 2-s AP trains, RRP size was estimated from the back-extrapolation (to time = 0) of average cumulative EPSP amplitudes recorded at 5 Hz (25) using Origin 8 "Pick Peaks" and "Interpolated Curve."

EPSPs with Low-frequency AP Trains—To measure the reduction of RRSVs in response to consecutive low-frequency AP firing, the EPSP amplitude recorded at 0.05 Hz or 0.2 Hz was normalized to the first EPSP amplitude or the mean EPSP amplitude from a 20-min recording before antibody injection (n = 5–7). To compare the rate of RRSVs reduction, the normalized and averaged amplitudes of EPSP were fitted with exponential curves using Origin 7.5 "Fit Exponential Decay with First Order or Second Order." The mean decay time constant was calculated from single exponential decay curves of individual EPSP recordings.

RRP Recovery from the Depletion—EPSP was recorded at 1 Hz. After a 1-min control recording at 1 Hz, a 4-min stimulation at 5 Hz was applied to deplete SVs in the RRP. To monitor EPSP amplitudes before, during, and after the 4-min train, the data-collecting software written by the late L. Tauc (Centre National de la Recherche Scientifique, Gif-sur-Yvette, France) was used.

A Moving Average Algorithm—EPSP amplitudes were normalized to the mean EPSP amplitudes before the 4-min train (n = 7–10) using Origin 8. Averaged EPSP amplitudes were smoothed using Origin 8 "5 Points Adjacent Averaging" to clearly show the increase in EPSP size.

Time Constant for RRP Recovery—Averaged EPSP amplitudes for each dynamin isoform knockdown (KD) were fitted with single exponential growth curves from 0 min to 0.14 min and 1.0 min or from 1 min to 6 min after the 4-min train using Origin 7.5 "Fit Exponential Growth." To clearly show the fast recovery rate, the mean value of noise level of the base line recording at time = 0, < 1 mV, was subtracted from the mean EPSP amplitudes, and the single exponential curves were normalized to the value at 0.45 min.

Statistics

Statistical significance was determined by two-tailed Student's t test or one-way ANOVA. All data are shown as the mean ± S.E. Statistical significance was assumed when $p < 0.05$. In figures, $^{*}p < 0.05$.

RESULTS

Expression and Knockdown of Dynamin Isoforms in SCG Neurons—We first confirmed the specificity of the commercially obtainable siRNAs against dynamin 1, 2, and 3 using HEK293T cells expressing each dynamin isoform (Fig. 1, *A* and *B*). Each siRNA inhibited corresponding dynamin expression selectively (Fig. 1*B*). We next confirmed the specificity of the commercially obtainable antibody against dynamin 1, 2, and 3 using whole brain extract (Fig. 1*C*) and a pheochromocytoma cell line, PC12 cells (Fig. 1*D*). All three isoforms in the brain (Fig. 1*C*) and PC12 cells (Fig. 1*D*) were detected by individual antibody against dynamin 1, 2, and 3. In addition, the specificity of siRNA against each dynamin was also confirmed in the PC12 cells (Fig. 1*D*).

We then attempted to quantify the expression of dynamin isoforms in SCG neurons in culture using the antibodies and siRNAs. However, we failed to perform quantitative Western blot analysis of dynamin isoforms or quantitative PCR because very low densities of SCG neurons are growing on high densities of glial cells for forming synapses between SCG neurons. Thus, using immunostaining, we examined the quantitative protein distribution of dynamin isoforms in SCG neurons and assessed their equivalent genetic knockdown by the siRNAs. Dynamin 1 is expressed in both the soma and neurites (Fig. 1*E*, *Dyn1*). The soma is occasionally surrounded by dynamin 1-expressing neurites (Fig. 1*E*, *lower panels*) of adjacent neurons (21–23). Similar to dynamin 1, dynamin 2 and 3 are detected by their specific antibody equivalently in SCG neurons in both the soma (Fig. 1*F*) and the surrounding neurites. To quantitatively assess the reduction of dynamin isoforms by each siRNA, the averaged fluorescence intensity of dynamin isoforms in three randomly chosen regions of 50 μm^2 each in the cytoplasm was normalized to the averaged value of regions from a non-injected neighboring neuron (Fig. 1, *F–H*). Dynamin isoform expression levels were not different between non-injected neurons and control siRNA-injected neurons (Fig. 1*F*), whereas each siRNA significantly reduced individual dynamin isoforms (Fig. 1*G*) within the standard range for reduction of protein level with siRNA KD (26, 27). Importantly, each isoform-specific siRNA did not reduce the expression levels of other dynamin isoforms (Fig. 1*H*), suggesting that knockdown of dynamin by each siRNA is selective and that individual dynamin siRNAs do not produce off-target effects.

Dynamin Isoforms Differentially Maintain Releasable Vesicle Pools—We next examined the relationship of dynamin to AP properties for the kinetics of vesicle recycling. Each of the three dynamin isoforms in presynaptic neurons was knocked down, and the recovery of RRSVs after evoked transmission was assessed with a paired-pulse protocol (Fig. 2*A*). EPSP amplitudes of the first recording were unchanged with a dynamin or a control siRNA transfection (Fig. 2*B*). Similar to non-trans-

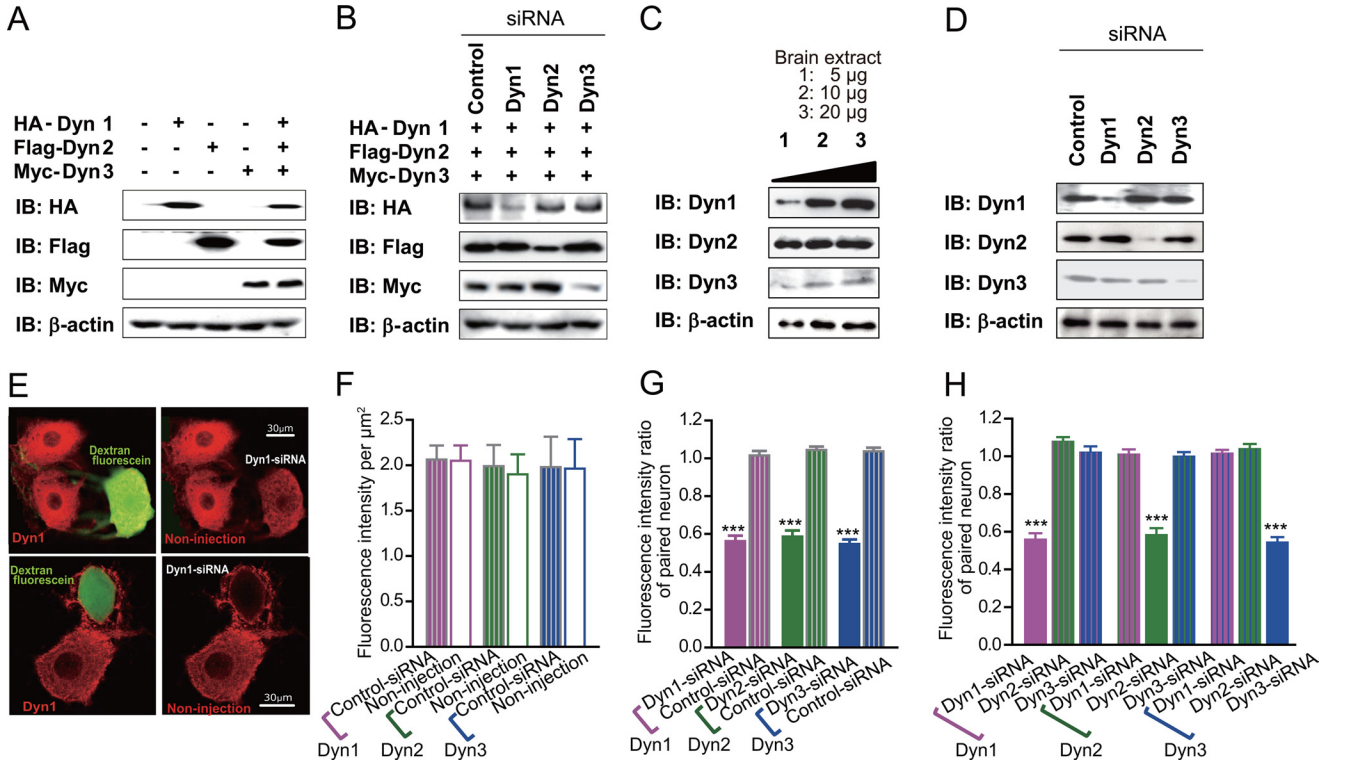

FIGURE 1. **Specificity of dynamin siRNAs and antibodies and knockdown of dynamin 1, 2, or 3 in SCG neurons.** *A* and *B*, dynamin isoforms transfected in HEK293T cells (*A*) and the reduction with siRNAs (*B*). HEK293T cells were transfected with 1 μg of MSCV-Puro-N-HA dynamin 1 (*HA-Dyn1*), MSCV-Puro-N-FLAG dynamin 2 (*FLAG-Dyn2*), or MSCV-Puro-N-Myc dynamin 3 (*Myc-Dyn3*) (*A*) with 100 pM of control siRNA, dynamin 1 (*Dyn1*), 2 (*Dyn2*) or 3 (*Dyn3*) siRNA (*B*). 48 h later, dynamin isoforms and β-actin as a control in the cell lysates were probed by the designated antibodies. *IB*, immunoblot. *C*, dynamin isoforms expression in brain. Dynamin isoforms and β-actin as a control in cell lysates prepared from rat brain were probed by the designated antibodies. *D*, dynamin isoform expression in PC12 cells and the reduction with siRNAs. PC12 cells were transfected with 100 pM of control siRNA, dynamin 1, 2, or 3 siRNA. Dynamin isoforms and β-actin as a control in cell lysates were probed by the designated antibodies. *E–H*, SCG neurons were injected with control, dynamin 1, 2, or 3 siRNA. *E*, *left panel*, immunofluorescence images of dynamin 1 (*red*) and dextran fluorescein (*green*), a marker for siRNA injection. *Right panel*, immunofluorescence images of dynamin 1 in non-injected neurons and neurons 3 days after injection with dynamin 1 siRNA. *F*, fluorescence intensity of dynamin 1, 2, or 3 in the cytoplasm injected with the control siRNA and an adjacently paired non-injected neuron (n = 6–17 pairs). *G* and *H*, fluorescence intensity of dynamin 1, 2, or 3 in the cytoplasm injected with control, dynamin 1, 2, or 3 siRNA was normalized to that of a paired, non-injected neuron (n = 11–22 pairs). ***, $p < 0.001$; unpaired Student's *t* test, control siRNA (*pink stripes*) *versus* dynamin 1 siRNA (*pink*), control siRNA (*green stripes*) *versus* dynamin 2 siRNA (*green*), and control siRNA (*blue stripes*) *versus* dynamin 3 siRNA (*blue*) (*G*); Bonferroni post hoc test after one-way ANOVA *versus* dynamin siRNAs (*H*). *F–H*, data are mean ± S.E.

fected neurons (Fig. 2*C*), synapses treated with control siRNA showed depression of the second EPSP (paired-pulse depression) at short ISIs (≤ 100 ms), whereas the amplitudes of the second EPSP were similar to that of the first EPSP at longer ISIs (≥ 100 ms) (Fig. 2, *C–F*). When dynamin 1, 2, or 3 were knocked down the second EPSP amplitude at longer ISIs (≥ 100 ms) was 60–70% that of control values (Fig. 2, *C–F*). With dynamin 1 KD, the paired-pulse depression for ISIs of 20 and 30 ms was similar to control values (Fig. 2*D*, the difference is not significant *versus* control but significant *versus* dynamin 3 KD), whereas dynamin 2 or 3 KD increased paired-pulse depression at short ISIs (20–100 ms) (Fig. 2, *E* and *F*). In contrast to the reduction of release probability observed in neurons from a dynamin 1 and 3 double knockout in highly active central neurons (28), it is unlikely that basal release probability is affected by dynamin loss of function in non-active SCG neurons in culture (21) because mean EPSP amplitudes of the first recording were unchanged with dynamin or a control siRNA transfection (Fig. 2*B*). Thus, in contrast to findings in central neurons of dynamin knockout mice (13, 15), in peripheral neurons, each dynamin isoform contributes equally to the regulation of rapid SV recycling for recovery of the RRP that occurs ≥ 50 ms after transmitter release is evoked by an AP. However, dynamin 1 does not appear to contribute significantly to rapid vesicle replenishment that occurs ≥ 20 ms of AP firing, suggesting an asymmetry in the involvement of dynamin isoforms in the major kinetic modes of SV recycling.

Distinct Roles of Dynamin Isoforms during High-frequency AP Firing—To further examine the relationship of individual dynamin isoforms to AP firing, their effect on the replenishment of RRSVs both during and after repetitive firing was examined. 2-s AP trains at 5, 10, and 20 Hz were applied every 2 min. We tested the frequencies of AP firing within the physiological range for sympathetic neurons (29) and avoided strong, non-physiological stimulation for sympathetic neurons, such as 10-s AP trains at 40 or 80 Hz that induce bulk endocytosis in central neurons (9). An AP train at a high frequency of 20 Hz induced synaptic depression (Fig. 3*A*, *Control*). In contrast with dynamin 1 KD, severe synaptic depression was extended to lower frequencies of 5 or 10 Hz in addition to 20 Hz (Fig. 3*A*, *Dyn1-KD*). In addition, at 2 min after a 5- or 10-Hz AP train, the recovery of the RRSVs from depression was impaired (Fig. 3*B*, *Dyn1-KD*), suggesting that dynamin 1 mediates SV membrane trafficking not only during but also after the AP train. With dynamin 2 KD, the recovery after a 10 Hz AP train was impaired weakly but significantly (Fig. 3*B*, *Dyn2-KD*). The reduction in

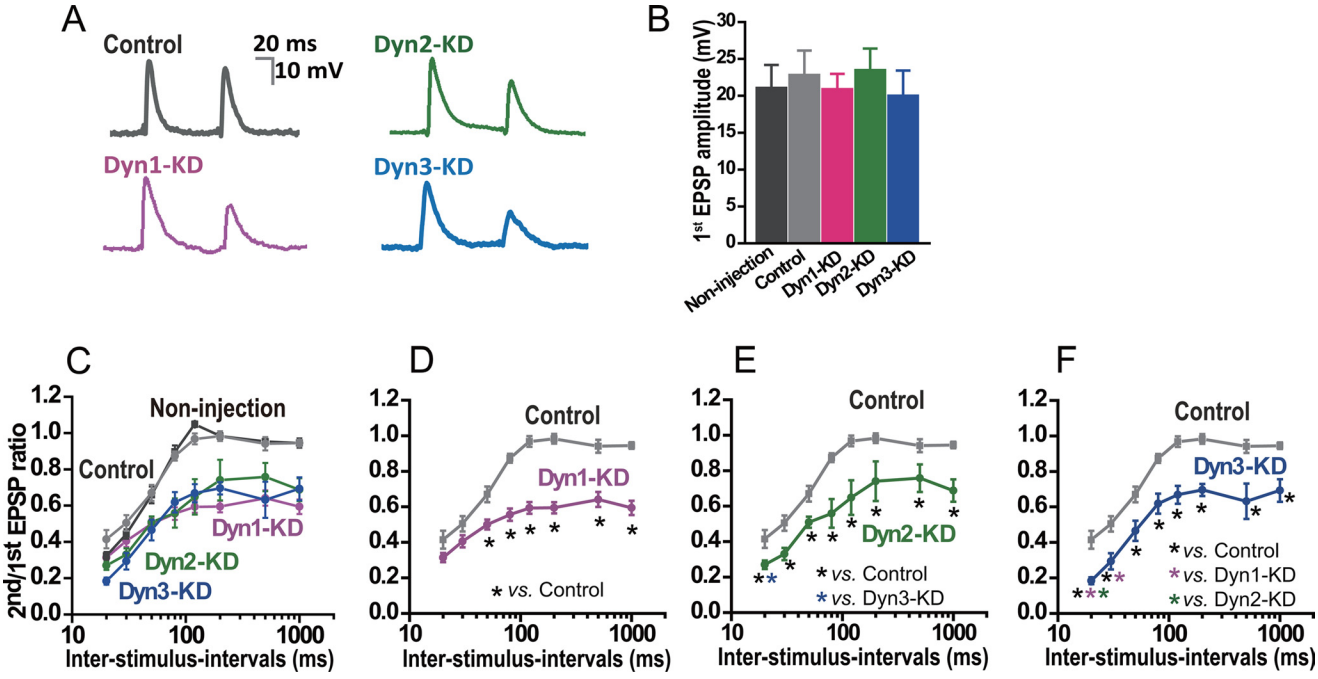

FIGURE 2. **Knockdown of dynamin 1, 2, or 3 reduces RRSVs after AP-evoked transmitter release.** Presynaptic neurons were injected with control or dynamin siRNA (*Control*, *Dyn1-KD*, *Dyn2-KD*, or *Dyn3-KD*). Changes in EPSP amplitude after an AP-evoked transmitter release were monitored by eliciting two consecutive APs at various ISIs, every 1 min, in an injected neuron. Three recordings for each ISI were performed ($n = 5–13$). *A*, EPSPs from a representative recording with an ISI of 120 ms. *B*, averaged amplitudes of the first EPSP with an ISI of 20 ms. $p > 0.05$, Bonferroni post hoc test after one-way ANOVA. *C–F*, the averaged paired-pulse ratio is plotted against the ISI. The control in *D–F* is same as the control siRNA data shown in *C* as *Control*. Dyn1-KD, Dyn2-KD, and Dyn3-KD in *D–F* are the same as the siRNA data shown in *C*. *, $p < 0.05$; unpaired Student's *t* test *versus* control (*gray*), dynamin 1 KD (*pink*), dynamin 2 KD (*green*), and dynamin 3 KD (*blue*). *B–F*, data are mean ± S.E.

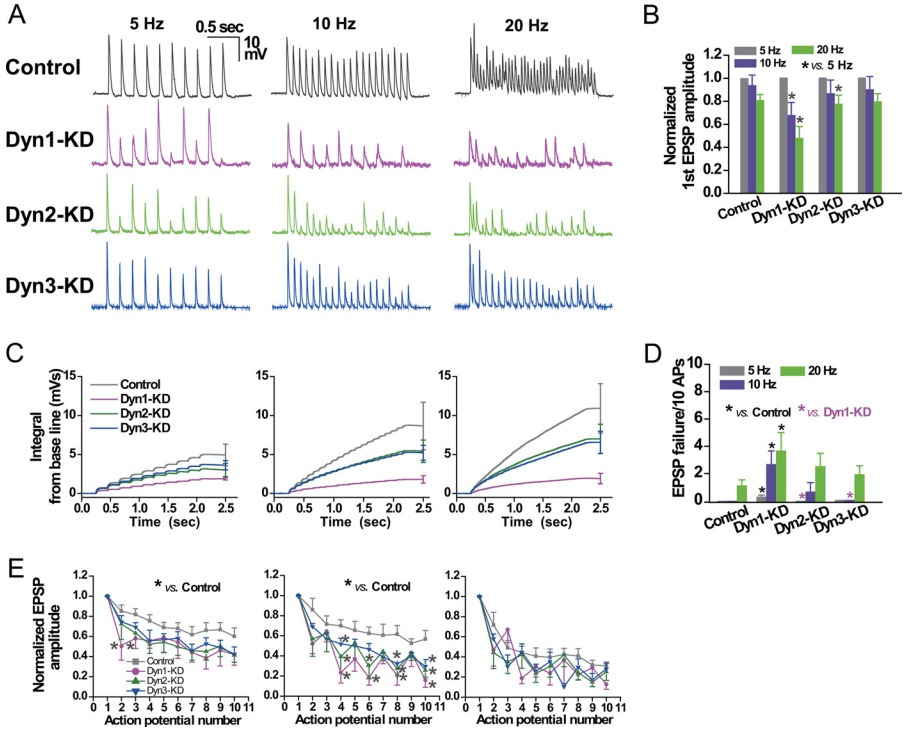

FIGURE 3. **Dynamin loss of function reduces RRSVs during and after high-frequency AP trains.** Presynaptic neurons were injected with control or dynamin siRNA (*Control*, *Dyn1-KD*, *Dyn2-KD*, or *Dyn3-KD*). 2-s AP trains at 5, 10, and 20 Hz were used to elicit EPSPs. Three recordings every 2 min were performed for each frequency ($n = 4–6$). *A*, EPSPs from representative consecutive recordings. *B*, amplitude of the first EPSP of each train normalized to the amplitude of the first EPSP in the 5-Hz train. *C*, averaged EPSP integral values calculated from regions over the base line of EPSP traces. *D*, number of EPSP failures during the first 10 APs of the 2-s train. *E*, the peak amplitude from the end of the previous EPSP was normalized to the first EPSP amplitude in each frequency train and averaged. *B–E*, data are mean ± S.E. *, $p < 0.05$; Bonferroni post hoc test after one-way ANOVA *versus* control (*gray*) and *versus* dynamin 1 KD (*pink*).

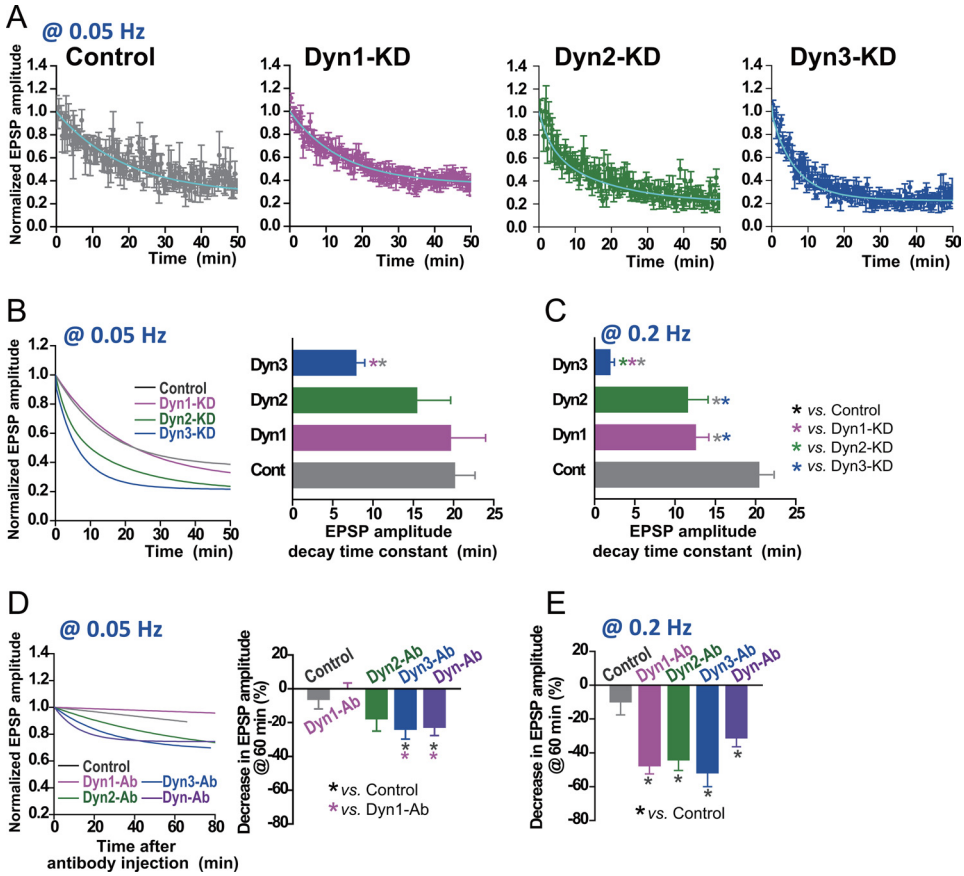

FIGURE 4. **Dynamin loss of function impairs RRSVs during low-frequency AP trains.** Presynaptic neurons were injected with control or dynamin siRNA (*Control*, *Dyn1-KD*, *Dyn2-KD*, and *Dyn3-KD*) (*A–C*) or were dialyzed with control IgG or antibody against each isoform of dynamin (*Control*, *Dyn1-Ab*, *Dyn2-Ab*, *Dyn3-Ab*, and *Dyn-Ab*) (*D* and *E*). The EPSP amplitude recorded at 0.05 Hz or 0.2 Hz was normalized to the first EPSP amplitude ($n = 5–7$) or the mean EPSP amplitude from the 20-min recording before antibody injection. *A*, averaged EPSP amplitudes with S.E. and the single exponential decay curve (*cyan*). *B*, *left panel*, single exponential decay curves shown in *A*. *B*, *right panel*, and *C*, the mean decay time constant calculated from single exponential decay curves of individual EPSP recordings, except for Dyn3-KD at 0.2 Hz showing the first mean decay time constant calculated from double exponential decay curves. *D*, *left panel*, averaged EPSP amplitudes were fitted with single exponential decay curves. *D*, *right panel*, and *E*, decrease in EPSP amplitudes 60 min after the start of antibody injection for 3 min. *, $p < 0.05$; Bonferroni post hoc test after one-way ANOVA *versus* control (*gray*), dynamin 1 KD (*pink*), dynamin 2 KD (*green*), and dynamin 3 KD (*blue*).

the EPSP integral (measured from the base line of the trace) suggests that dynamin 1 KD reduced the number of RRSVs to 20–25% of control values following 2-s AP trains at 10 and 20 Hz (Fig. 3*C*). It is unlikely that the RRP size before the AP train was affected by dynamin loss of function because the number of SVs in the RRP (estimated from the back-extrapolation (to time = 0) of cumulative EPSP amplitudes recorded at 5 Hz) (25) was unchanged with dynamin 1, 2, 3 (118, 117, 118 SVs), or control siRNA injection (111 SVs). Surprisingly, dynamin 1 KD increased the number of EPSP failures during 2-s trains at 5–20 Hz (Fig. 3, *A* and *D*). These results suggest that dynamin 1 mediates SV recycling during high levels of synaptic activity. The time course of the reduction in peak amplitude of the first ten EPSPs in a 5- or 10-Hz train, but not a higher frequency such as 20 Hz that induces Ca^{2+} channel-mediated synaptic depression in controls (19, 30), was comparable during knockdown of each dynamin isoform (Fig. 3*E*), suggesting that all three isoforms can drive SV recycling during the train. Together, these results suggest that each dynamin isoform contributes to maintenance of the RRP *via* replenishment of SVs during high frequency firing and that dynamin 1 and 2 mediate longer-lasting SV recycling after high-frequency firing.

Distinct Roles of Dynamin Isoforms during Low-frequency AP Firing—We next examined the involvement of different dynamin isoforms in setting the time window for SV replenishment following AP firing, monitoring the recovery kinetics of RRSVs during low-frequency synaptic activity consisting of consecutive presynaptic APs at 0.05 or 0.2 Hz. The EPSP gradually depressed over the 50-min recording session (Fig. 4*A*, *Control*). The time constant for the reduction of RRSVs was estimated by fitting the mean EPSP amplitudes with an exponential decay curve (Fig. 4, *A–C*). Dynamin 1 KD showed a more rapid reduction in EPSP than control levels of depression following repetitive APs at 0.2 Hz but not at 0.05 Hz (Fig. 4, *B* and *C*). In contrast, dynamin 3 KD accelerated the reduction in EPSP at both firing rates. The decay time constant with dynamin 3 KD was significantly faster than that with control, dynamin 1 KD, or dynamin 2 KD (Fig. 4*B*, *right panel*, and *C*). The EPSP amplitude was decreased with dynamin 3 KD at both firing rates, whereas it was decreased with dynamin 1 KD at 0.2 Hz but not 0.05 Hz (Fig. 4, *B* and *C*), suggesting an activity-dependent action for dynamin 1. Dynamin 2 KD caused more rapid decreases in EPSP amplitude at the higher frequency (Fig. 4, *B* and *C*). These results were consistent with those of

dynamin dysfunction induced by dialysis of isoform-specific antibodies (Fig. 4, *D* and *E*). Dynamin or dynamin 3 specific antibody rapidly decreased the EPSP amplitude at 0.05 and 0.2 Hz, whereas dynamin 1 or 2 antibody caused a larger decrease in EPSP amplitude at the higher frequency. In addition, dialysis of the dynamin 1 antibody into the presynaptic neuron transfected with dynamin 1 siRNA caused no further decrease in EPSP amplitude (data not shown), suggesting that the siRNA and the antibody used in this study are specific. Together, our results demonstrate that, at low-frequency firing, dynamin 1-mediated SV replenishment is activated at 0.2 Hz, or within 5 s after AP generation, whereas dynamin 3-mediated SV replenishment is activated at lower than 0.05 Hz and takes more than 20 s, in a firing rate-independent manner, and dynamin 2 exhibits dual properties.

Dynamin Isoforms Have Distinct Roles in Vesicle Pool Recovery Kinetics—We next asked how the different dynamin isoforms contribute to SV recycling pathways with distinct kinetics. We showed previously that, after depletion of the RRP, the SV pool recovers at two time constants, fast and slow, through distinct pathways (Fig. 5, *A* and *B*) (24). Here, to map dynamin isoform specificity onto the fast and slow components, we applied the same recovery protocol. The recovery of RRSVs following full depletion of the RRP due to a train of 4-min APs at 5 Hz was monitored by measuring the EPSP amplitude every 1 s (Fig. 5, *B–F*). To determine the effect of dynamin on fast and slow recovery, we measured EPSP amplitudes at 10 s (end of the fast recovery) and 6 min (during the slow recovery) after cessation of the AP train (Fig. 5, *G* and *H*). Each dynamin KD appeared to prevent recovery in both cases (Fig. 5, *B–F*). However, reduction in the EPSP amplitude is significant for dynamin 1 or 2 KD at 10 s and for dynamin 3 KD at 6 min. These results suggest dynamin isoform specificity on the fast and slow components.

Therefore, we next analyzed the kinetics associated with each dynamin isoform in the regulation of the fast and slow SV recycling pathways. We compared recovery time constants with exponential growth curves fitted to the increase in the mean EPSP amplitude by 7.8 s (Fig. 5*I*), 60 s (Fig. 5, *J* and *L*), and 1–6 min (Fig. 5, *K* and *M*). For control, the time constant for the fast recovery to 60 s was $\tau = 3.6 \pm 0.3$ s (Fig. 5, *J* and *L*), and the slow recovery to 6 min was 70 ± 12 s (Fig. 5, *K* and *M*) ($n = 11$). Dynamin 3 KD showed a time constant for fast recovery similar to the control value (Fig. 5*L*), and dynamin 1 KD showed a time constant for slow recovery similar to the control value (Fig. 5*M*), whereas the degree of recovery was much less than the control (Fig. 5, *L* and *M*). In contrast, the recovery rate of the fast phase was delayed with dynamin 1 or 2 KD (Fig. 5*L*), and the recovery rate of the slow phase was delayed with dynamin 2 or 3 KD, respectively (Fig. 5*M*). To obtain a clearer comparison of the recovery rates, exponential curves for the fast recovery rate were normalized to 0.5 min (Fig. 5*N*), and the slow recovery rate was normalized to 6 min (Fig. 5*O*). The normalized exponential curves indicate significant delays for dynamin 1 KD (Fig. 5*N*) and dynamin 3 KD (Fig. 5*O*), respectively. In contrast, dynamin 2 KD showed a delay in both the fast and slow rates of recovery (Fig. 5, *N* and *O*). Thus, a kinetic analysis using normalization suggests dynamin isoform specificity for fast and slow recycling pathways.

The contribution of individual isoforms to the fast and slow components was confirmed in a dynamin 1, 2, and 3 triple KD that resulted in effects similar to single KD, reducing recovery of the EPSP amplitude (Fig. 5, *F–H*) and delaying both the fast and slow rates of recovery (Fig. 5, *L–O*). Together, these results suggest that each of the three dynamin isoforms have a distinct relationship to fast and slow SV recycling pathways to replenish a common RRSV pool but with an interactive and not an additive effect. In addition, the severely delayed EPSP recovery, even in the presence of the other two isoforms (Fig. 5, *C–E*), also suggests a non-additive relationship between dynamin isoforms. To confirm this further, we estimated the actual contribution of dynamin 1, 2, and 3 for the RRP recovery (Fig. 5*P*). The estimated recovery is 20% smaller at the end of fast recovery and 25% smaller at 6 min during slow recovery (Fig. 5*P*), suggesting that both phases of recovery are under the influence of additional factors (16, 24, 31, 32). However, although these additional factors appear to be involved in the control of RRP recovery rates for fast and slow pathways (Fig. 5*P*), dynamin 1 mainly regulates the replenishment of RRP with a rapid rate for the selective recovery of SV depletion during and after high-frequency stimulation (Figs. 3 and 6). In contrast, dynamin 3 mainly regulates RRP replenishment at a slow rate, mediating a separate endocytic pathway that is independent of AP frequency (Figs. 4 and 6). Finally, consistent with its hybrid properties in AP firing, dynamin 2 contributes approximately equally to both fast and slow pathways. However, remarkably, the degree of participation of dynamin 2 in supporting the fast or slow pathways appears to be determined by the particular firing frequency of the neuron (Figs. 3, 4, and 6).

DISCUSSION

In this study, we address the fundamental issue of how the SV recycling machinery can adapt to wide variations in AP frequency. Our overall findings indicate that dynamin isoforms together cover the range of AP frequency patterns for the selection of specific vesicle reuse modes that replenish a shared RRP (Fig. 6). Replenishment of the RRP *via* a dynamin 1-mediated pathway occurred both during and after high-frequency AP firing (0.2–20 Hz) with a latency of 0.05 s after AP generation. In contrast, dynamin 3-mediated a separate mode of RRP replenishment that was independent of AP frequency and activated rapidly ($\leq$0.02 s) after AP generation. A third response mode was observed for dynamin 2, which contributed to both pathways. Thus, with three mammalian isoforms, dynamin appears to provide complete coverage of SV recycling pathways required to respond to the full physiological range of AP firing patterns that may be generated by neurons *in vivo*.

This study is the first to assign roles of the three dynamin isoforms to replenishment of a shared SVs release pool in response to variations in AP firing. Furthermore, our findings suggest that the cells have intrinsic mechanisms to control the temporal window for vesicle pool replenishment (Fig. 6). In the case of sympathetic neurons, AP activates RRP replenishment via dynamin 1 with a latency of 0.05 s (Fig. 2*D*) and lasting 5 s (Fig. 4*C*), whereas dynamin 2 and 3 activation occurs with a

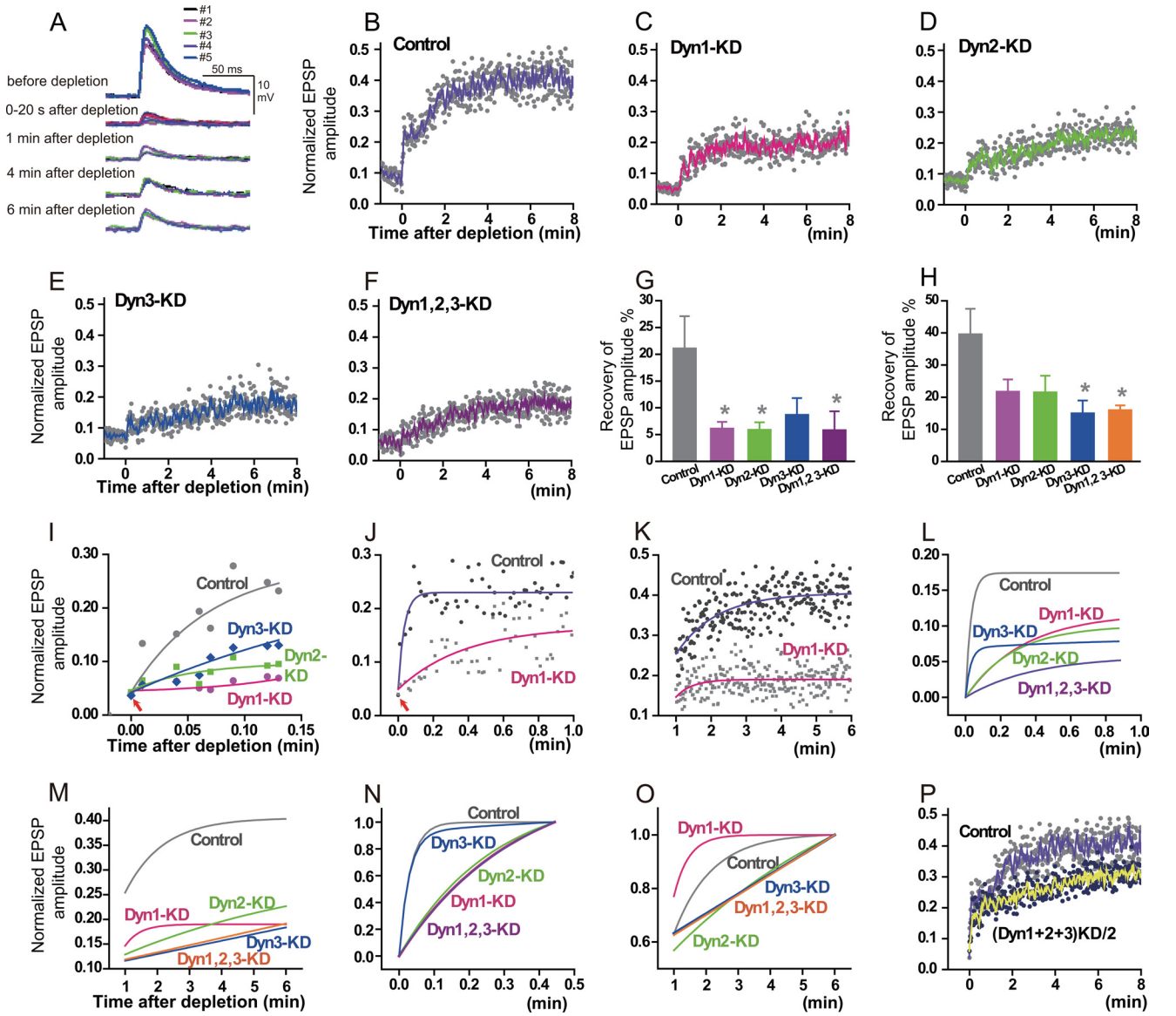

FIGURE 5. **Dynamin loss of function delays the recovery of RRSVs.** Presynaptic neurons were injected with control or dynamin siRNA (*Control*, *Dyn1-KD*, *Dyn2-KD*, *Dyn3-KD*, or *Dyn1,2,3-KD*). The recovery of RRSVs in a neuron with dynamin KD was monitored by measuring the amplitude of EPSP recorded at 1 Hz (*B–E*). After a 1-min control recording at 1 Hz, a 4-min stimulation at 5 Hz was applied to deplete SVs in the RRP. EPSP amplitudes were normalized to the mean EPSP amplitudes before the 4-min train. *A*, as a control, representative EPSP traces in a non-transfected synapse from consecutive 10-s recordings before and 1 min, 4 min, and 6 min after the depleting stimulation of a 4-min AP train at 5 Hz and 20-s recordings after the depleting stimulation. The recording at 0 s after the depleting stimulation is the base line, eliciting no EPSP. An EPSP trace was recorded at 0.5 Hz. *B–F*, averaged EPSP amplitudes plotted with the *smoothed lines* using a moving average algorithm ($n = 7–10$). *G* and *H*, recovery of EPSP amplitudes at 10 s (*G*) and 6 min (*H*) after the depleting stimulation. Data are mean ± S.E. *, $p < 0.05$; Bonferroni post hoc test after one-way ANOVA *versus* control. *I–K*, increase in averaged EPSP amplitudes and the single exponential growth curves for each dynamin isoform KD by 8 s (*I*) and for dynamin 1 KD by 1 min (*J*) and 1–6 min (*K*) after the depleting stimulation. The averaged EPSP amplitudes are same as shown in *B–E*. *L* and *M*, single exponential growth curves for each dynamin isoform KD calculated from averaged EPSP amplitudes shown in *B–F* and *J–K*. The noise level value of the base line eliciting no EPSP at time = 0 shown in *I* and *J* with *arrows* is subtracted from the mean EPSP amplitudes for the fitting. *N* and *O*, the single exponential curves shown in *L* and *M* were normalized to the value at 0.45 min (*N*) or at 6 min (*O*). *P*, the values shown in *C–E* were added, and the resultant values were divided by 2. The values estimating contributions of all three isoforms were plotted and fitted with a *smoothed line* (*yellow*) using a moving average algorithm. The control value is the same as the control values shown in *B*. The averaged noise level value of the base line eliciting no EPSP at time = 0 shown in *I* and *J* with *arrows* is subtracted.

faster, 0.02 s latency (Fig. 2, *E* and *F*), lasting 5 s (Fig. 4*C*) and 20 (Fig. 4*B*) to 120 s (Fig. 3*B*), respectively. During and after high-frequency but not low-frequency firing, dynamin 1 and 2 activation is prolonged, whereas dynamin 3 activation is independent of firing frequency (Fig. 3*B*). After RRP depletion, dynamin 1 and 2 mediate recovery with fast kinetics ($\tau < 3.6$ s), whereas dynamin 2 and 3 mediate recovery with slow kinetics ($\tau < 70$ s) (Fig. 5). The fast process corresponds to rapid RRP refilling with SVs from the RP in an amphiphysin-dependent endocytic pathway, whereas the slow process involves a gradual refilling of the RRP with SVs through an amphiphysin-independent endocytic pathway that bypasses the RP (24). Loss of function of specific dynamin isoforms slowed the RRP recovery through the amphiphysin-dependent endocytic pathway, suggesting that dynamin isoforms control not only the kinetics but also the size of the RP. During and after high-frequency AP firing, a reduction in the size of RRP may accelerate the amphiphysin-dependent endocytic pathway to fill the RP, resulting in recovery of

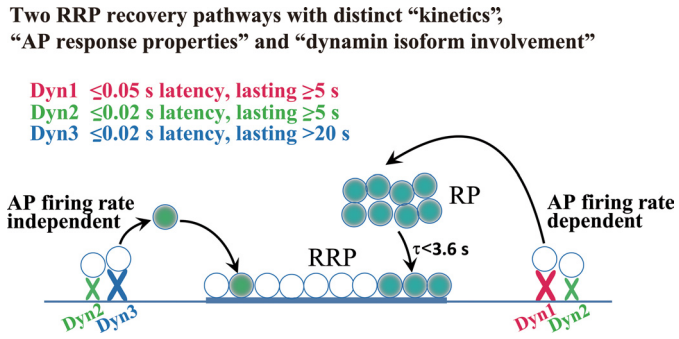

FIGURE 6. **Two RRP recovery pathways with distinct kinetics, AP response properties, and dynamin isoform involvement.** After an AP, dynamin 1-mediated recovery occurs in a slow time window of 0.05 s (Fig. 2), lasting 5 s (Fig. 4), whereas dynamin 2- and 3-mediated recovery occurs in a fast, 0.02-s window (Fig. 2) lasting 5 s and more than 20 s (Fig. 4), respectively. During and after high-frequency firing, dynamin 1- and 2-mediated recovery lasts longer than 5 s (Fig. 4), whereas dynamin 3-mediated recovery is independent of firing frequency (Fig. 4). The AP firing rate-dependent pathway allows RRP recovery faster ($\tau < 3.6$ s) than the AP firing rate-independent pathway ($\tau <$ 70 s) (Fig. 5, *J* and *K*). Both recovery pathways are not additive and, therefore, are likely to be influenced by additional scaling factors (20–25%, Fig. 5*P*).

the base line RRP size. Our results suggest that the AP firing drives the recovery process due to the pattern of AP firing. Thus, it is critical to have two pathways that can each respond to firing variation patterns to replenish the RRP.

The speed of endocytosis, ranging from hundreds of milliseconds to hundreds of seconds, has been estimated by capacity measurements and synaptophluorin imaging (1). In contrast to fast endocytosis, a more rapid time window of tens of milliseconds suggests a role for dynamin in the clearance of endocytic vesicle cargo from active zones. A requirement (< 0.02 s after an AP) for rapid dynamin action in SV membrane trafficking and active zone clearance has been proposed for the *Drosophila shibire* mutant (17) and at the calyx of Held after dynamin dysfunction (16), respectively. Our study suggests that, with three isoforms, two of them gating distinct kinetic response pathways and the third isoform shared between the two and contingent on firing pattern, the dynamin endocytosis system appears well positioned to manage replenishment of the RRP with SVs under a range of physiological AP firing patterns encountered by neurons *in vivo*. Studies at the calyx of Held (16, 33) indicate that rapid dynamin action may be the rate-limiting step for RRP replenishment, suggesting that dynamin isoforms may be crucial regulatory control points for the response of the membrane to cell activity. Indeed, in our study, dynamin knockdown impaired the ability of cells to translate high-frequency AP firing into recovery and maintenance of the RRP (Figs. 3 and 5). In addition, the number (31) and the position (32) of exocytosis events may also affect RRP recovery rates (Fig. 5).

Collectively, our findings provide a foundation for understanding the molecular mechanisms responsible for the selection and regulation of distinct membrane trafficking complexes by electrical activity. We propose the novel idea that distinct dynamin isoforms controlling unique vesicle pools may allow synapses to dynamically respond to rapid or complex APs bursts into EPSPs that reflect a history of synaptic firing of a cell while simultaneously maintaining the general capability for fast and stable SV recycling and maintenance after sparse single APs. Whether there is a spatial synaptic organization to dynamin isoform-dependent recycling pathways remains a challenging future issue.

Acknowledgments—We thank Dr. Charles T. Yokoyama and Dr. Gary J. Stephens for comments on the manuscript. We also thank Dr. Eriko Aizu-Yokota for technical assistance with PC12 cell preparation.

REFERENCES

1. Wu, L. G. (2004) Kinetic regulation of vesicle endocytosis at synapses. *Trends Neurosci.* **27,** 548–554
2. Ceccarelli, B., Hurlbut, W. P., and Mauro, A. (1973) Turnover of transmitter and synaptic vesicles at the frog neuromuscular junction. *J. Cell Biol.* **57,** 499–524
3. Heuser, J. E., and Reese, T. S. (1973) Evidence for recycling of synaptic vesicle membrane during transmitter release at the frog neuromuscular junction. *J. Cell Biol.* **57,** 315–344
4. Royle, S. J., and Lagnado, L. (2003) Endocytosis at the synaptic terminal. *J. Physiol.* **553,** 345–355
5. Kuromi, H., and Kidokoro, Y. (2002) Selective replenishment of two vesicle pools depends on the source of Ca^{2+} at the *Drosophila* synapse. *Neuron* **35,** 333–343
6. Artalejo, C. R., Henley, J. R., McNiven, M. A., and Palfrey, H. C. (1995) Rapid endocytosis coupled to exocytosis in adrenal chromaffin cells involves Ca^{2+}, GTP, and dynamin but not clathrin. *Proc. Natl. Acad. Sci. U.S.A.* **92,** 8328–8332
7. Zhang, Q., Li, Y., and Tsien, R. W. (2009) The dynamic control of kiss-and-run and vesicular reuse probed with single nanoparticles. *Science* **323,** 1448–1453
8. Clayton, E. L., Evans, G. J., and Cousin, M. A. (2008) Bulk synaptic vesicle endocytosis is rapidly triggered during strong stimulation. *J. Neurosci.* **28,** 6627–6632
9. Wu, L. G., Ryan, T. A., and Lagnado, L. (2007) Modes of vesicle retrieval at ribbon synapses, calyx-type synapses, and small central synapses. *J. Neurosci.* **27,** 11793–11802
10. Wenzel, E. M., Morton, A., Ebert, K., Welzel, O., Kornhuber, J., Cousin, M. A., and Groemer, T. W. (2012) Key physiological parameters dictate triggering of activity-dependent bulk endocytosis in hippocampal synapses. *PLoS ONE* **7,** e38188
11. Takei, K., McPherson, P. S., Schmid, S. L., and De Camilli, P. (1995) Tubular membrane invaginations coated by dynamin rings are induced by GTP-γ S in nerve terminals. *Nature* **374,** 186–190
12. Cao, H., Garcia, F., and McNiven, M. A. (1998) Differential distribution of dynamin isoforms in mammalian cells. *Mol. Biol. Cell* **9,** 2595–2609
13. Ferguson, S. M., Brasnjo, G., Hayashi, M., Wölfel, M., Collesi, C., Giovedi, S., Raimondi, A., Gong, L. W., Ariel, P., Paradise, S., O'Toole, E., Flavell, R., Cremona, O., Miesenböck, G., Ryan, T. A., and De Camilli, P. (2007) A selective activity-dependent requirement for dynamin 1 in synaptic vesicle endocytosis. *Science* **316,** 570–574
14. Cook, T. A., Urrutia, R., and McNiven, M. A. (1994) Identification of dynamin 2, an isoform ubiquitously expressed in rat tissues. *Proc. Natl. Acad. Sci. U.S.A.* **91,** 644–648
15. Raimondi, A., Ferguson, S. M., Lou, X., Armbruster, M., Paradise, S., Giovedi, S., Messa, M., Kono, N., Takasaki, J., Cappello, V., O'Toole, E., Ryan, T. A., and De Camilli, P. (2011) Overlapping role of dynamin isoforms in synaptic vesicle endocytosis. *Neuron* **70,** 1100–1114
16. Hosoi, N., Holt, M., and Sakaba, T. (2009) Calcium dependence of exo- and endocytotic coupling at a glutamatergic synapse. *Neuron* **63,** 216–229
17. Kawasaki, F., Hazen, M., and Ordway, R. W. (2000) Fast synaptic fatigue in shibire mutants reveals a rapid requirement for dynamin in synaptic vesicle membrane trafficking. *Nat. Neurosci.* **3,** 859–860
18. Mochida, S., Westenbroek, R. E., Yokoyama, C. T., Itoh, K., and Catterall, W. A. (2003) Subtype-selective reconstitution of synaptic transmission in sympathetic ganglion neurons by expression of exogenous calcium channels. *Proc. Natl. Acad. Sci. U.S.A.* **100,** 2813–2818
19. Mochida, S., Few, A. P., Scheuer, T., and Catterall, W. A. (2008) Regulation

of presynaptic $Ca_V2.1$ channels by Ca^{2+} sensor proteins mediates short-term synaptic plasticity. *Neuron* **57,** 210–216
20. Mochida, S. (2011) Activity-dependent regulation of synaptic vesicle exocytosis and presynaptic short-term plasticity. *Neurosci. Res.* **70,** 16–23
21. Mochida, S., Nonomura, Y., and Kobayashi, H. (1994) Analysis of the mechanism for acetylcholine release at the synapse formed between rat sympathetic neurons in culture. *Microsc. Res. Tech.* **29,** 94–102
22. Krapivinsky, G., Mochida, S., Krapivinsky, L., Cibulsky, S. M., and Clapham, D. E. (2006) The TRPM7 ion channel functions in cholinergic synaptic vesicles and affects transmitter release. *Neuron* **52,** 485–496
23. Mochida, S., Kobayashi, H., Matsuda, Y., Yuda, Y., Muramoto, K., and Nonomura, Y. (1994) Myosin II is involved in transmitter release at synapses formed between rat sympathetic neurons in culture. *Neuron* **13,** 1131–1142
24. Lu, W., Ma, H., Sheng, Z. H., and Mochida, S. (2009) Dynamin and activity regulate synaptic vesicle recycling in sympathetic neurons. *J. Biol. Chem.* **284,** 1930–1937
25. Schneggenburger, R., Meyer, A. C., and Neher, E. (1999) Released fraction and total size of a pool of immediately available transmitter quanta at a calyx synapse. *Neuron* **23,** 399–409
26. Su, Q., Cai, Q., Gerwin, C., Smith, C. L., and Sheng, Z. H. (2004) Syntabulin is a microtubule-associated protein implicated in syntaxin transport in neurons. *Nat. Cell Biol.* **6,** 941–953
27. Ying, Y., Li, L., Cao, W., Yan, D., Zeng, Q., Kong, X., Lu, L., Yan, M., Xu, X., Qu, J., Su, Q., and Ma, X. (2012) The microtubule associated protein syntabulin is required for glucose-stimulated and cAMP-potentiated insulin secretion. *FEBS Lett.* **586,** 3674–3680
28. Lou, X., Fan, F., Messa, M., Raimondi, A., Wu, Y., Looger, L. L., Ferguson, S. M., and De Camilli, P. (2012) Reduced release probability prevents vesicle depletion and transmission failure at dynamin mutant synapses. *Proc. Natl. Acad. Sci. U.S.A.* **109,** E515–523
29. Libet, B., and Mochida, S. (1988) Long-term enhancement (LTE) of postsynaptic potentials following neural conditioning, in mammalian sympathetic ganglia. *Brain Res.* **473,** 271–282
30. Leal, K., Mochida, S., Scheuer, T., and Catterall, W. A. (2012) Fine-tuning synaptic plasticity by modulation of $Ca_V2.1$ channels with Ca^{2+} sensor proteins. *Proc. Natl. Acad. Sci. U.S.A.* **109,** 17069–17074
31. Zhu, Y., Xu, J., and Heinemann, S. F. (2009) Two pathways of synaptic vesicle retrieval revealed by single-vesicle imaging. *Neuron* **61,** 397–411
32. Park, H., Li, Y., and Tsien, R. W. (2012) Influence of synaptic vesicle position on release probability and exocytotic fusion mode. *Science* **335,** 1362–1366
33. Haucke, V., Neher, E., and Sigrist, S. J. (2011) Protein scaffolds in the coupling of synaptic exocytosis and endocytosis. *Nat. Rev. Neurosci.* **12,** 127–138